The current issue and full text archive of this journal is available at
www.emeraldinsight.com/0961-5539.htm

Received September 2004
Revised August 2005
Accepted November 2005

Transient mixed convective heat transfer predictions around three heated cylinders in a horizontal channel

Horng-Wen Wu
Department of System and Naval Mechatronic Engineering, National Cheng Kung University, Tainan, Taiwan, Republic of China

Shiang-Wuu Perng
Department of Accounting Information, Kun Shan University of Technology, Tainan, Taiwan, Republic of China

Sheng-Yuan Huang
Department of System and Naval Mechatronic Engineering, National Cheng Kung University, Tainan, Taiwan, Republic of China, and

Tswen-Chyuan Jue
Department of Vehicle Engineering, National Formosa University, Yunlin, Taiwan, Republic of China

Abstract

Purpose – To investigate the effect of transient mixed convective flow interaction between circular cylinders and channel walls on heat transfer with three circular cylinders arranged in an isosceles right-angled triangle within a horizontal channel.

Design/methodology/approach – This paper uses a semi-implicit finite element method to solve the incompressible Navier-Stokes equation, energy equation and continuity equation in primitive-variable form by assuming the flow to be two-dimensional and laminar.

Findings – Provides information indicating that the transient streamlines, isotherms, drag coefficient and time-mean Nusselt number around the surfaces of three cylinders are affected by various gap-to-diameter ratio, Reynolds numbers and Grashof numbers. The results show that the maximum value of surface- and time-mean Nusselt number along cylinders exists at $S = 0.75$.

Research limitations/implications – It is limited to two-dimensional laminar flow for the transient mixed convective flow interaction between circular cylinders and channel walls in a horizontal channel.

Practical implications – A very useful source of information and favorable advice for people is applied to heat exchangers, space heating, power generators and other thermal apparatus.

Originality/value – The results of this study may be of interest to engineers attempting to develop thermal control of thermal apparatus and to researchers interested in the flow-modification aspects of mixed convection between circular cylinders and channel walls in a horizontal channel.

Keywords Convection, Fluid power cylinders, Flow

Paper type Research paper

International Journal of Numerical Methods for Heat & Fluid Flow
Vol. 16 No. 6, 2006
pp. 674-692

0961-5539
DOI 10.1108/09615530610679057

The authors gratefully acknowledge the partially financial support of the National Council of the Republic of China for the present work.

Nomenclature

$A_{\alpha\beta}$ = diffusion matrix of energy
C_d = drag coefficient
D = cylinder diameter
d = distance between cylinder and geometric center (Figure 1)
F_d = drag force
Gr = Grashof number $(g\beta(T^*_W - T^*_\infty)D^3)/(\nu^2)$
g = gravity acceleration
H = channel wall-to-wall distance
$H_{\alpha\beta}$ = pressure gradient matrix
$K_{\alpha\beta\gamma j}$ = conduction matrix
L = channel length
$M_{\alpha\beta}$ = mass matrix
N_i = shape function of four nodal points
Nu = Nusselt number $(-\partial\Theta/\partial n)$
$\overline{Nu}$ = time-mean Nusselt number
$\overline{Nu}_{avg}$ = surface- and time-mean Nusselt number
n = outer normal vector
P = dimensionless pressure difference $(P^*/\rho u^2_\infty)$
P_i = P^* of node i
P^* = the difference between pressure and hydrostatic pressure
Pr = Prandtl number (ν/α)
Re = Reynolds number $(u_\infty D/\nu)$
r = radial coordinate
S = gap-to-diameter ratio (d/D)
$S_{\alpha i\beta j}$ = diffusion matrix of the momentum equation
T^* = temperature
T^*_w = wall temperature
T^*_∞ = uniform inlet temperature
t = dimensionless time $(t^*/(D/u_\infty))$
t_p = the duration of a period
t^* = time
u_∞ = uniform inlet velocity
u, v = dimensionless velocity components $(u = u^*/u_\infty, v = v^*/u_\infty)$
u_i = velocity components $(u_1 = u, u_2 = v)$
u_t = dimensionless tangential velocity
$u^* v^*$ = velocity components
$u_{\alpha i}$ = velocity components of node α
$\hat{u}_{\alpha i}$ = intermediate velocity components of node α
x, y = dimensionless $x^* y^*$ coordinates $(x = x^*/D, y = y^*/D)$
$x^* y^*$ = physical coordinates
α = thermal diffusivity of fluid
Θ = dimensionless temperature $\left((T^* - T^*_\infty)/(T^*_w - T^*_\infty)\right)$
Θ_w = dimensionless wall temperature
θ = plane angle
ρ = density of fluid
ν = kinematic viscosity of fluid
Σ_α = surface integration in energy equation
δ_{i1} = Kronecker delta
Δt = time step

Superscripts

$n + 1$, n, $n - 1$ $n + 1$th, nth, $n - 1$th time step

1. Introduction

Mixed convection heat transfer around circular cylinders has been applied to heat exchangers, space heating, power generators and other thermal apparatus. In these applications, it is required to analyze the influence of flow interaction between multiple cylinders on mixed convective heat transfer (Zdravkovic, 1994).

For a circular cylinder, if the Reynolds number is sufficiently large, vortex shedding will occur in the wake. This vortex shedding can affect the heat transfer characteristics of a cylinder (Žukauskas and Žiugžda, 1985). However, the combined wake behind multiple cylinders is different from that behind an isolated circular cylinder. The research on the wake behind three circular cylinders is not as much as on single circular cylinder and two circular cylinders. Chou and Chao (1991) investigated experimentally the flow interaction for a staggered configuration of three circular cylinders by changing the longitudinal distance and lateral spacing at a Reynolds number of 500, based on the diameter of a single cylinder. Lam and Cheung (1988)

presented how the flows around three circular cylinders arranged in an equidistant triangular cluster interact at different angles of incidence and spacing ratios. Igarashi (1993) carried out experimental studies to predict the aerodynamic forces on three cylinders composed of a main cylinder and two sub-cylinders closely arranged in line. They indicated that the flow patterns were changed by the reattachment of the separated shear layer from the upstream cylinder to the downstream cylinder. Inoue and Hattori (2003) presented a numerical study of combined forced and natural convection heat transfer in a bundle of cylinders arranged in an equilateral triangular pattern. Their results showed that the reverse flows appear along the center line in the sub-channel with increasing Richardson number.

There are a few studies done on the influence of flow interaction between multiple cylinders on heat transfer in confining walls. Kundu *et al.* (1991) used the stream function-vorticity approach to simulate laminar flow and heat transfer over a row of in-line cylinders placed between two parallel plates. They showed that both values of the spacing between cylinders and the distance between plates control the shape and appearance of standing vortices and the shedding of vortices. Those distinct streamlines and vortex patterns determined the heat transfer to the flow. Gowda *et al.* (1997) numerically simulated mixed convection heat transfer over in-line bundles of cylinders in a vertical duct. The effect of Richardson number on the flow and heat transfer has been studied. Horibe *et al.* (1995) conducted an experimental work on the forced convection heat transfer characteristics of three cylinders formed across at a Reynolds number of 4.6×10^4 in which the effects of the distance between the cylinders and its axial variation on the heat-transfer characteristics of the second cylinder were extensively determined. Lacroix and Carrier (1995) presented a numerical study of mixed convection heat transfer around two vertically separated horizontal cylinders within confining adiabatic walls. The paper investigated the effect of the cylinder spacing, of the distance between the parallel plates, and the Gr/Re^2 ratio on the heat transfer and fluid flow. Jue *et al.* (2001) predicted numerically the heat transfer of transient mixed convective flow around three heated cylinders between two vertical parallel plates.

Since, the direction of buoyancy effect is orthogonal to the direction of fluid flow for a horizontal channel (Wu and Perng, 1999; Kim *et al.*, 1992), the effect of buoyancy effect on flow and heat transfer for a horizontal channel must be different from that for a vertical channel where the direction of buoyancy effect is parallel to the direction of fluid flow. Besides, flow past circular cylinders placed with their axis normal to the flow can be assumed to be two-dimensional flow, when the cylinders are so long compared with their diameter that their ends have no effect (Tritton, 1988). A low Reynolds number flow regime ($Re < 2{,}300$) exists in very compact heat exchangers (Kundu *et al.*, 1991) or the decay heat removal by natural circulation of coolant for a liquid metal fast breeder reactor (Inoue and Hattori, 2003), so the flow can be laminar. Since, three circular cylinders can be used as a unit for the heat exchangers, the purpose of this paper is to investigate the effect of flow interaction among three circular cylinders arranged in an isosceles right-angled triangle on heat transfer in a horizontal channel by assuming the flow to be two-dimensional and laminar. This paper uses a semi-implicit finite element method (Ramaswamy and Jue, 1992) to solve the incompressible Navier-Stokes equations, energy equation and continuity equations in primitive-variable form.

2. Problem description

The problem considered in this study is a viscous, incompressible and transient mixed convection flow passing across three heated cylinders within a horizontal channel as shown in Figure 1. The geometrical relationships are set as $L/D = 20$, $H/D = 6$, and $S = d/D = 0.5, 0.75, 1.0, 1.25$. The distance from the inflow boundary to the front of cylinder A is H and that from the outflow boundary to the rear of cylinder B or cylinder C is $L - (H + d + 3D/2)$. The center of cylinder A is located on the axial line of the channel, and then the center of cylinder B is located at $(5D - 2d)/2$ from the top wall and cylinder C also at $(5D - 2d)/2$ from the bottom wall. As d increases with an increase in S, cylinder B is closer to the top wall and cylinder C closer to the bottom wall, too.

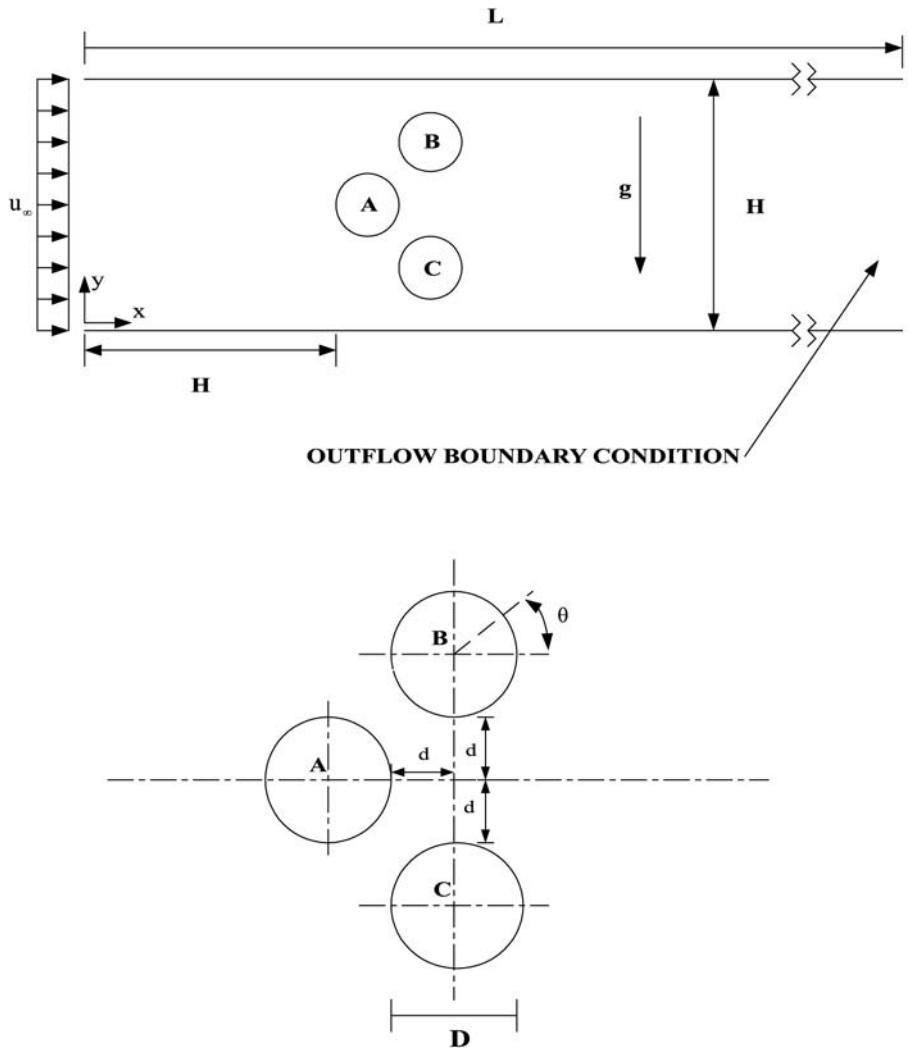

Figure 1.
Flow configuration for computation

3. Formulation and numerical methods

The governing equations consist of continuity equation, Navier-Stokes equations and energy equation formulated in terms of velocity, pressure and temperature. Let Ω be a bounded domain in R^2, and τ be a positive real value. The spatial and temporal coordinates are denoted by $x_i \in \Omega$ and $t \in [0, \tau]$. Under the Boussinesq approximation (Tritton, 1988), these equations, expressed in dimensionless form, are:

$$u_{i,i} = 0 \quad \text{in } \Omega \tag{1}$$

$$\frac{\partial u_i}{\partial t} + u_j u_{i,j} = -P_{,i} + \frac{1}{Re}(u_{i,j}u_{j,i})_{,j} + \frac{Gr}{Re^2}\Theta\delta_{i1} \quad \text{in } \Omega \tag{2}$$

$$\frac{\partial \Theta}{\partial t} + u_j \Theta_{,j} = \frac{1}{Re\,Pr}\Theta_{,jj} \quad \text{in } \Omega \tag{3}$$

where $u_1 = u$, $u_2 = v$

The initial conditions are:

$$u_1 = u_2 = \Theta = 0, \quad \text{in the region, for } t = 0 \tag{4}$$

The boundary conditions used for computations are given as follows: uniform inflow with $u = 1$, $v = 0$; no-slip boundary conditions on the upper and lower channel surfaces and on the cylinder surfaces. The traction free condition is imposed at the outflow boundary as proposed by Ramaswamy and Jue (1992). The temperature field satisfies $\Theta = 0$ at the inflow boundary, $\Theta = 1$ along the cylinder (heat-producing) surfaces, and $\partial\Theta/\partial n = 0$ along the other surfaces.

The variables are interpolated by using a four-node quadrilateral element as:

$$u_i = \sum_{\alpha=1}^{4} N_\alpha u_{\alpha i}, \quad P = \sum_{\alpha=1}^{4} N_\alpha P_\alpha, \quad \Theta = \sum_{\alpha=1}^{4} N_\alpha \Theta_\alpha \tag{5}$$

where N_α is the shape function.

Applying the standard Galerkin finite element to the spatial discretization of equations (1)-(3) yields nonlinear simultaneous ordinary differential equations of the form Ramaswamy and Jue (1992):

$$H_{\alpha i\beta} u_{\beta i} = 0 \tag{6}$$

$$M_{\alpha\beta}\frac{\mathrm{d}u_{\beta i}}{\mathrm{d}t} + H_{\alpha i\beta}P_\beta + \frac{1}{Re}S_{\alpha i\beta j}u_{\beta j} + K_{\alpha\beta\gamma j}u_{\beta j}u_{ji} = \frac{Gr}{Re^2}M_{\alpha\beta}\Theta_\beta\delta_{i1} \tag{7}$$

$$M_{\alpha\beta}\frac{\mathrm{d}\Theta_\beta}{\mathrm{d}t} + \frac{1}{Re\,Pr}A_{\alpha\beta}\Theta_\beta + K_{\alpha\beta\gamma j}u_{\beta j}\Theta_\gamma = \frac{1}{Re\,Pr}\Sigma_\alpha \tag{8}$$

where:

$$H_{\alpha i\beta} = \int_\Omega (N_{\alpha,i}N_\beta)\mathrm{d}\Omega \tag{9}$$

$$M_{\alpha\beta} = \int_\Omega (N_\alpha N_\beta)\mathrm{d}\Omega \tag{10}$$

$$S_{\alpha i\beta j} = \int_{\Omega} (N_{\alpha,i} N_{\beta,j}) \mathrm{d}\Omega \tag{11}$$

$$K_{\alpha\beta\gamma j} = \int_{\Omega} (N_{\alpha} N_{\beta,j} N_{\gamma}) \mathrm{d}\Omega \tag{12}$$

$$A_{\alpha\beta} = \int_{\Omega} (N_{\alpha,j} N_{\beta,j}) \mathrm{d}\Omega \tag{13}$$

$$\Sigma_{\alpha} = \int_{\Gamma} (N_{\alpha} \Theta_{,j}) n_j \mathrm{d}\Gamma \tag{14}$$

By adopting a second-order Adams-Bashforth scheme for the advection terms and an implicit Euler representation for the diffusion term, we may derive the finite element version of the semi-implicit projection scheme as follows (Ramaswamy and Jue, 1992).

Step 1. Advection and viscosity phase. In the phase, intermediate velocities $\hat{u}_i^{n+1}$ are found from u_i^n beginning with u_0 for $n = 0$, using the explicit Adams-Bashforth method for the nonlinear convective terms and a first-order implicit Euler time integration scheme for the diffusion term:

$$\begin{aligned} M_{\alpha\beta}\hat{u}_{\beta i}^{n+1} = M_{\alpha\beta}u_{\beta i}^{n} - \Delta t\left(\frac{3}{2}K_{\alpha\beta\gamma j}u_{\beta j}^{n}u_{\gamma i}^{n} - \frac{1}{2}K_{\alpha\beta\gamma j}u_{\beta j}^{n-1}u_{\gamma i}^{n-1}\right) \\ - \frac{\Delta t}{Re}S_{\alpha i\beta j}\hat{u}_{\beta j}^{n+1} + \frac{\Delta t Gr}{Re^2}M_{\alpha\beta}\Theta_{\beta}^{n}\delta_{i1} \end{aligned} \tag{15}$$

Step 2. Pressure phase. The phase allows us to determine final velocities u_i^{n+1} from intermediate velocities $\hat{u}_i^{n+1}$ by adding the dynamic effect of the pressure P^{n+1} so that the incompressibility condition stays satisfied. This leads to the Poisson equation:

$$A_{\alpha\beta}P_{\beta}^{n+1} = -\frac{1}{\Delta t}H_{\alpha i\beta}\hat{u}_{\beta i}^{n+1} \tag{16}$$

The final velocities are:

$$M_{\alpha\beta}^{D}u_{\beta i}^{n+1} = M_{\alpha\beta}^{D}\hat{u}_{\beta i}^{n+1} - \Delta t H_{\alpha i\beta}P_{\beta}^{n+1} \tag{17}$$

where $M_{\alpha\beta}^{D}$ denotes the diagonalized mass matrix obtained simply by summing across each row of the consistent mass matrix and placing the results in the diagonal.

Step 3. Temperature phase. In the last phase, temperature Θ^{n+1} is found by the energy equation as the way in the velocity phase is derived:

$$\begin{aligned} M_{\alpha\beta}\Theta_{\beta}^{n+1} = M_{\alpha\beta}\Theta_{\beta}^{n} - \Delta t\left(\frac{3}{2}K_{\alpha\beta\gamma j}u_{\beta j}^{n}\Theta_{\gamma i}^{n} - \frac{1}{2}K_{\alpha\beta\gamma j}u_{\beta j}^{n-1}\Theta_{\gamma i}^{n-1}\right) \\ - \frac{\Delta t}{Re\,Pr}A_{\alpha\beta}\Theta_{\beta}^{n+1} + \frac{\Delta t}{Re\,Pr}\Sigma_{\alpha}^{n} \end{aligned} \tag{18}$$

The element mass, convection, pressure gradient, divergence, and diffusion matrices are calculated only once and used again at each time step. The skyline method was used to reduce the storage of global matrices. A direct solver of LU factorization based on Gaussian elimination technique was developed to deal with a symmetric banded system. For forced convection ($Re = 100$-300) and mixed convection ($Gr = 80{,}000$ and 200,000) with $Pr = 0.7$, the gap-to-diameter ratio (S) is changed by 0.5, 0.75, 1.0, and 1.25 to investigate the effect of the gap between cylinders on unsteady flow and heat transfer. After a series of mesh sensitivity test for three finite-element meshes (5,646 nodes and 5,424 elements, 7,380 nodes and 7,118 elements, 8,930 nodes and 8,643 elements), the calculation results are showed in Figure 2. It is found that the time-mean Nusselt number difference between the second and the third mesh less than 0.05 percent in test runs, so a finite-element mesh (7,380 nodes and 7,118 elements) was chosen for all cases. It was 8,000 time steps with $\Delta t = 0.005$ required to produce periodic vortex shedding and the computation time was from 1 h 11 m 21 s to 1 h 37 m 52 s of CPU time in a PENTIUM III 1G PC, depending on the physical case.

4. Relevant physical parameters

Drag coefficient. The pressure and viscous forces on the surface of the cylinder in x-direction are given by definition of the drag force; that is:

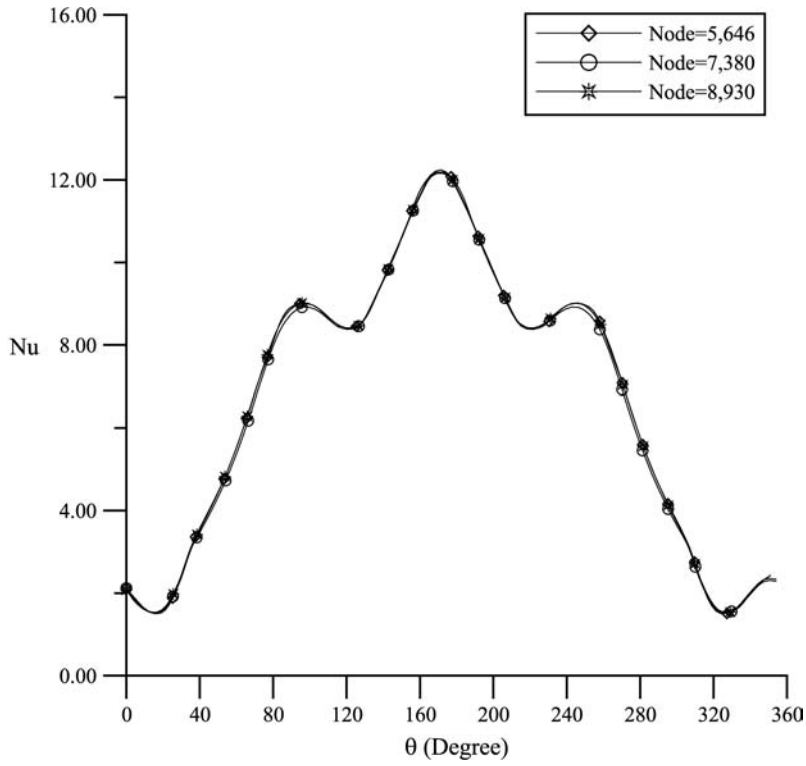

Figure 2.
Mesh sensitivity test

$$F_{\mathrm{d}} = \int_0^{2\pi} (P^*)(\cos\theta) r \mathrm{d}\theta + \int_0^{2\pi} \tau_{\mathrm{w}}^* (\sin\theta) r \mathrm{d}\theta$$

The drag coefficient is expressed as:

$$C_{\mathrm{d}} = \frac{F_{\mathrm{d}}}{(1/2)\rho u_\infty^2 D} = \frac{2\int_0^{2\pi} P(\cos\theta) r \mathrm{d}\theta}{D} + \frac{\frac{2}{Re}\int_0^{2\pi} \frac{\partial u_t}{\partial n}(\sin\theta) r \mathrm{d}\theta}{D}$$

where $\partial u_t / \partial n$ denotes the dimensionless gradient of tangential velocity in the direction normal to the cylinder surface.

Nusselt number. From the balance of heat flux at the surface, the Nusselt number can be obtained as:

$$Nu = -\frac{\partial \Theta}{\partial n}$$

The time-mean Nusselt number is defined as:

$$\overline{Nu} = \frac{\int_0^{t_{\mathrm{P}}} Nu \mathrm{d}t}{t_{\mathrm{P}}}$$

The surface-and time-mean Nusselt is then written as:

$$\overline{Nu}_{\mathrm{avg}} = \frac{1}{2\pi} \int_0^{2\pi} \overline{Nu} \mathrm{d}\theta$$

5. Results and discussion

Since, there were no reports found to deal with three cylinders in a horizontal channel presented here, we apply the present method to solve the unsteady flow of laminar mixed convection from a cylinder within vertical confining walls before solving the problem. The cylinder is considered to be at a uniform temperature, and the channel walls are considered to be isothermal as inlet fluid temperature. The values of time-mean Nusselt number shown in Figure 3 agreeing well with Nakabe *et al.*'s (1996) result give one confidence in the use of the present solution scheme.

The time-mean Nusselt number along the surfaces of three cylinders is shown in Figure 4 for forced convection ($Re = 200$) at $S = 0.5$. For cylinder A, the maximum Nusselt number occurs at the front stagnation point on the cylinder ($\theta = 180°$); the minimum value occurs at the rear stagnation point on the cylinder ($\theta = 0°$). For cylinder B, the maximum Nusselt number occurs at $\theta = 226°$; the minimum value occurs at $\theta = 44°$ instead of the rear stagnation point on the cylinder. For cylinder C, the maximum Nusselt number occurs at $\theta = 133°$; the minimum value also occurs at $\theta = 316°$ instead of the rear stagnation point on the cylinder. These results can be explained from Figure 5(a). For cylinder A, the curvature of the streamline becomes large locally at the front stagnation point; this has a high flow velocity, so the convective heat transfer is large. There is a recirculation zone behind the rear stagnation point. The flow and wake is symmetric for cylinder A, so that the distribution of time-mean Nusselt number along the cylinder is also symmetric about

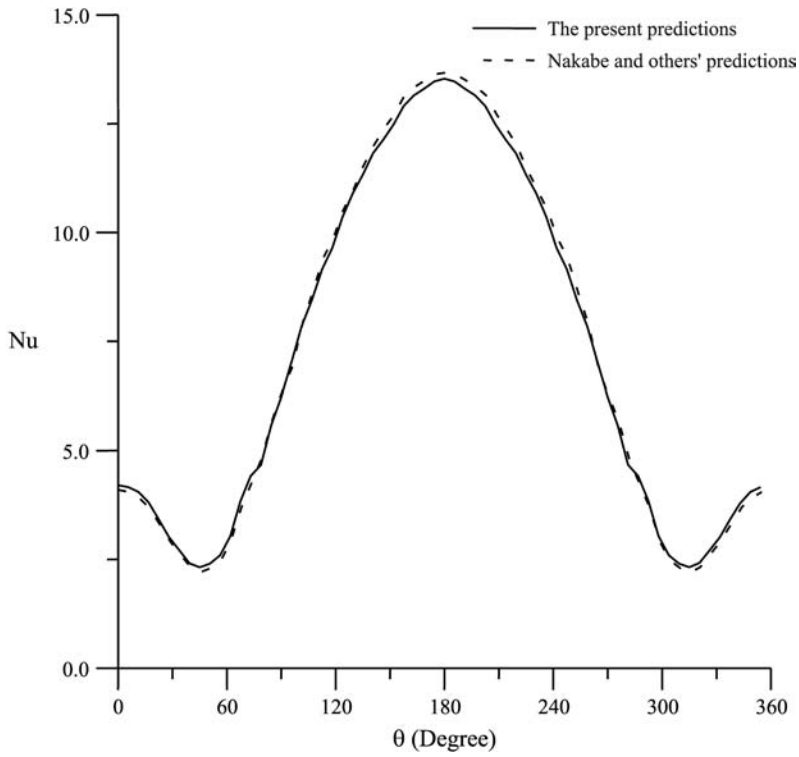

Figure 3.
Comparison between the present predictions and Nakabe and others' predictions for $Re = 120$ ($Gr = 1440$, $D/H = 0.3$)

the front stagnation point (Figure 4). The wake for upstream cylinder A spreads sideways restricted by the narrow gap effect between downstream cylinders B and C, and the effect induces the fluid flow toward downstream to form a jet flow along the gap between cylinders A and B and between cylinders A and C. This flow can be locally accelerated to enhance heat transfer around $\theta = 226°$ for cylinder B and around $\theta = 133°$ for cylinder C. Vortex shedding takes place behind cylinders B and C, and wave flows being formed move to the downstream flow. This phenomenon improves heat transfer at the rear stagnation points on cylinders B and C from a comparison with that point on cylinder A (Figure 4). The isotherms for forced convection ($Re = 200$) at $S = 0.5$ are shown in Figure 6(a). For cylinder A, the isotherms near the front stagnation point ($\theta = 180°$) are closer than those at any other position; in contrast, for cylinder B and C, the isotherms at $\theta = 226$ and 133°, respectively, are closer than those at any other position. Closer isothermal lines indicate a higher temperature gradient and accordingly a higher value of Nusselt number. Figure 7 shows the time-mean Nusselt number along the surfaces of three cylinders for forced convection ($Re = 200$) at $S = 1.0$. For all the three cylinders, the maximum Nusselt number occurs at $\theta = 180°$ and the distributions of Nusselt number for cylinders B and C have the same values from $\theta = 132$ to 210° while they have different values in other locations due to the interaction between the oscillating recirculation zones behind cylinders B and C. The values of maximum Nusselt number on cylinders B and C at $S = 1.0$ are smaller than those on cylinders B and C at $S = 0.5$, because the fluid between the cylinders A

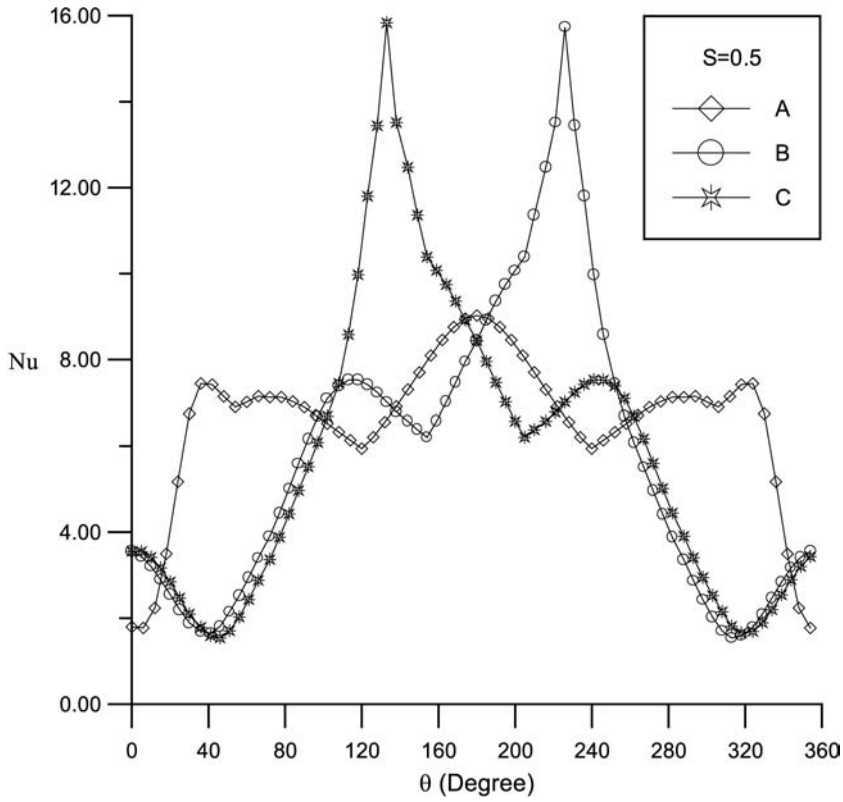

Figure 4.
Time-mean Nusselt number profiles around three cylinders for forced convection ($Re = 200$) at $S = 0.5$

and B and between the cylinders A and C are decelerated for a larger value of S due to the action of shear flow (Figure 5(b)). At $S = 1.0$, the shear-layer flow for the triple-cylinder configurations is so strong as to have a symmetric distribution of Nusselt number (Figures 5(b) and 7). Owing to a larger gap between cylinders A and B and between cylinders A and C, the shear-layer flow occurs instead of jet flow to increase the momentum in the gap. Therefore, the value of maximum Nusselt number on cylinder A at $S = 1.0$ is larger than that on cylinder A at $S = 0.5$. The isotherms for forced convection ($Re = 200$) at $S = 1.0$ are shown in Figure 6(b). For all the three cylinders, the isotherms near the front stagnation point ($\theta = 180°$) are closer than any other position. The drag coefficients for cylinders with forced convection ($Re = 200$) at $S = 1.0$ are shown in Figure 8. It can be seen that the unsteady flow is a periodic motion. The values of drag coefficient for cylinder A are smaller than for cylinders B and C because they are closer to the wall and have obvious vortex shedding.

In Figure 9, the time-mean Nusselt number along the surfaces of three cylinders at $S = 0.5$ for $Re = 200$ and $Gr = 200{,}000$ has obvious differences from that for forced convection ($Re = 200$). For cylinder A, the distribution of time-mean Nusselt number along the surface of cylinder is not symmetric about the front stagnation point ($\theta = 180°$). It is due to that the direction of buoyancy effect is orthogonal to the direction of fluid flow through a channel. From Figure 10(a), the non-symmetric flow

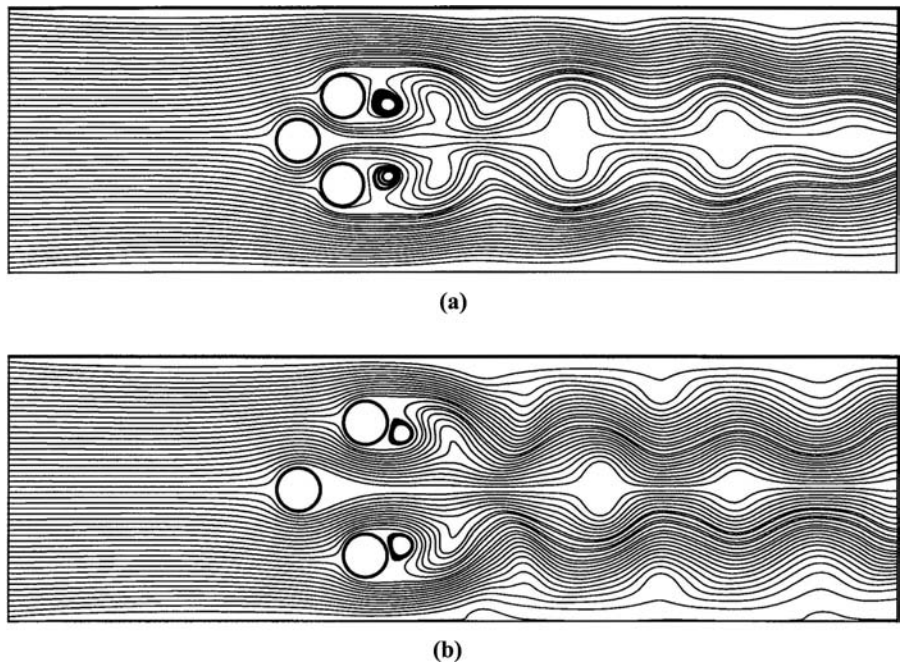

Figure 5.
Streamlines for forced convection ($Re = 200$): (a) $S = 0.5$ (b) $S = 1.0$ (each time at the peak point of one vortex-shedding cycle)

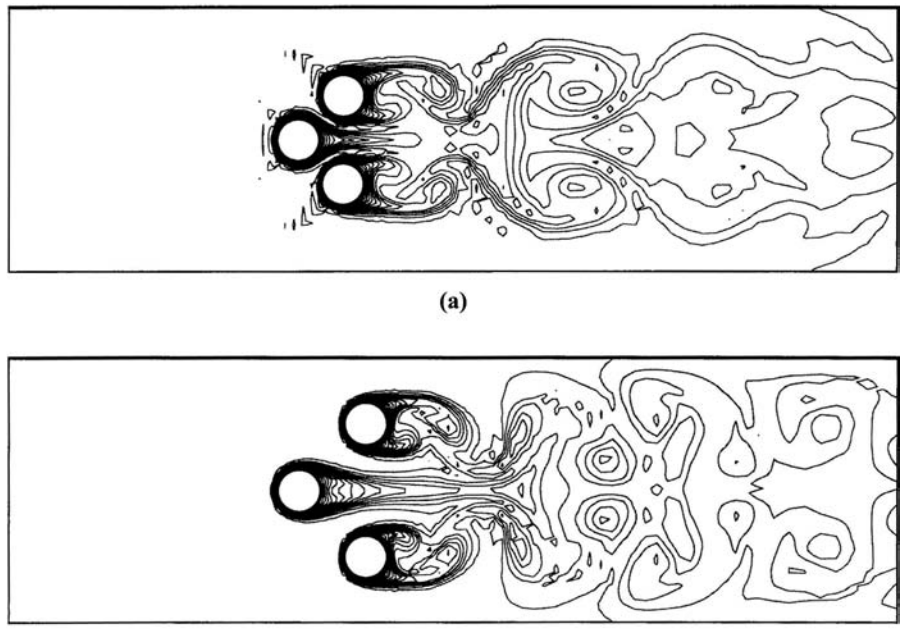

Figure 6.
Isotherms for forced convection ($Re = 200$): (a) $S = 0.5$ (b) $S = 1.0$ (each time at the peak point of one vortex-shedding cycle)

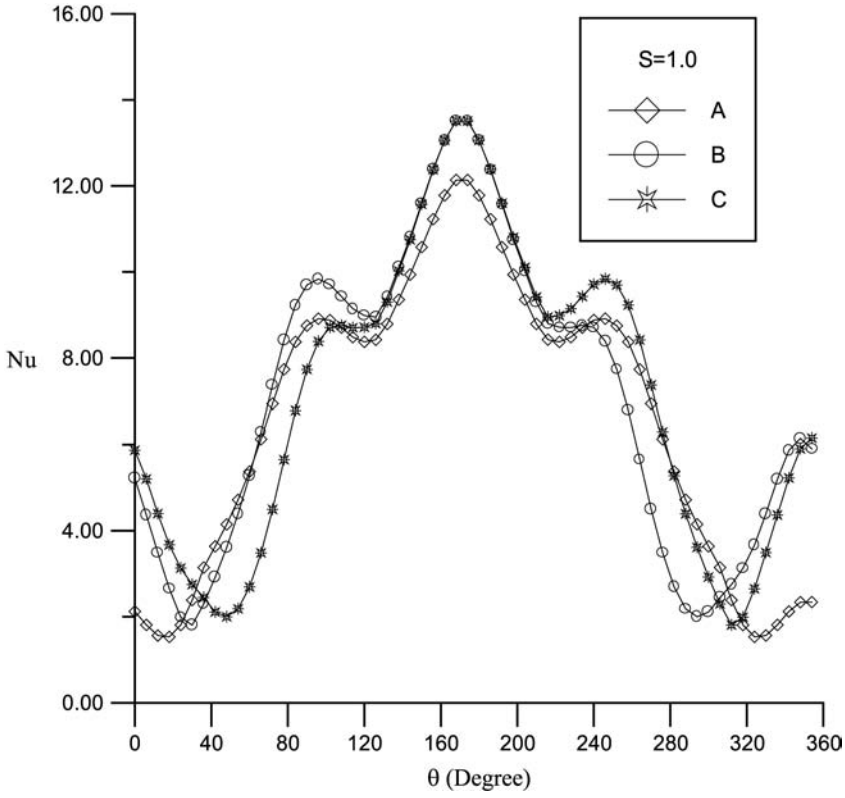

Figure 7.
Time-mean Nusselt number profiles around three cylinders for forced convection ($Re = 200$) at $S = 1.0$

patterns about the front stagnation of cylinder A have been seen obviously and two vortices have formed along the lower channel-wall because of upward buoyancy effect. Besides, the unsteady vortices behind cylinders B and C have the tendency toward the upper-right surfaces of cylinders. Furthermore, wave flows behind cylinders B and C are more obvious than for forced convection ($Re = 200$). From a comparison of Figures 9 and 4, it can be seen that the location of the maximum Nusselt number for cylinder A shifts to 46° and the locations of the minimum Nusselt number for cylinders B and C shift to $\theta = 56$ and 76°, respectively. The maximum values of Nusselt number along the surfaces of cylinders A and C for $Re = 200$ and $Gr = 200{,}000$ are larger than for forced convection ($Re = 200$), because of upward buoyancy effect on the cylinders A and C. Besides, owing to upward buoyancy effect, the angles which occur at the minimum Nusselt number have the tendency toward the angles located on the upper-right surfaces of cylinders B and C (Figure 9). The isotherms for $Re = 200$ and $Gr = 200{,}000$ at $S = 0.5$ and 1.0 are shown in Figure 11. The positions of closest isotherms around three cylinders are almost the same as those for forced convection ($Re = 200$), but both patterns behind cylinders are non-symmetric about the front stagnation of cylinder A and have a trend to be upward due to the upward buoyancy effect. Figure 12 shows the time-mean Nusselt number along surfaces of three cylinders for $Re = 200$ and $Gr = 200{,}000$ at $S = 1.0$. At $S = 1.0$, the profiles of time-mean

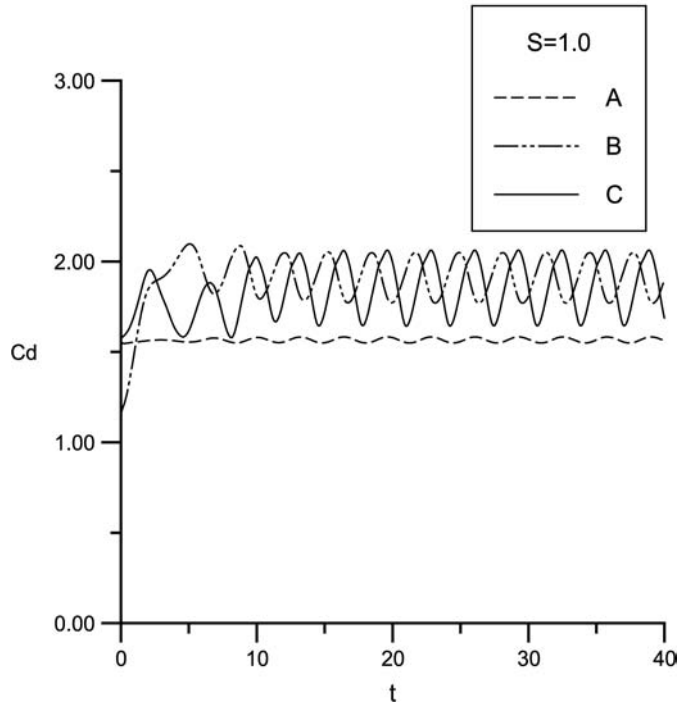

Figure 8.
Drag coefficient C_d vs time for forced convection ($Re = 200$) at $S = 1.0$

Nusselt number along the surfaces of three cylinders for $Re = 200$ and $Gr = 200{,}000$ have the distributions similar to those for forced convection ($Re = 200$) except that the locations of the minimum Nusselt number for cylinders B and C change to $\theta = 44$ and 62°, respectively, and the peak values of time-mean Nusselt number are larger than those for forced convection ($Re = 200$). From $\theta = 128$ to 217° the distributions of Nusselt number for cylinders A and B almost have the same values, but the result is different from that for forced convection (Figure 7). This difference between Figures 7 and 12 is caused by the non-symmetric flow patterns resulting from the upward buoyancy effect. The buoyancy effect can change the flow pattern as shown in Figure 10(b) from a comparison with Figure 5(b). Therefore, the non-symmetric flow patterns about the front stagnation of cylinder A exist, and there is a reversal that includes two vortices along the downstream location near the lower channel-wall as shown in Figure 10(b). At $S = 1.0$, the unsteady vortices behind cylinders B and C have the tendency toward the upper-right surfaces of cylinders, and the two flow reversals which occur along the lower channel-wall at $S = 0.5$ are merged into a bigger reversal including two vortices. Owing to the larger gap between cylinders, more increasing transport in momentum in the gap makes the reversal bigger. The curves of drag coefficients versus time for cylinders are shown in Figure 13 at $S = 1.0$ for $Re = 200$ and $Gr = 200{,}000$. From a comparison of Figure 13 with Figure 8, the cyclic variations in Figure 13 are no more simple-harmonic and have larger amplitudes than those in Figure 8 because of upward buoyancy effect.

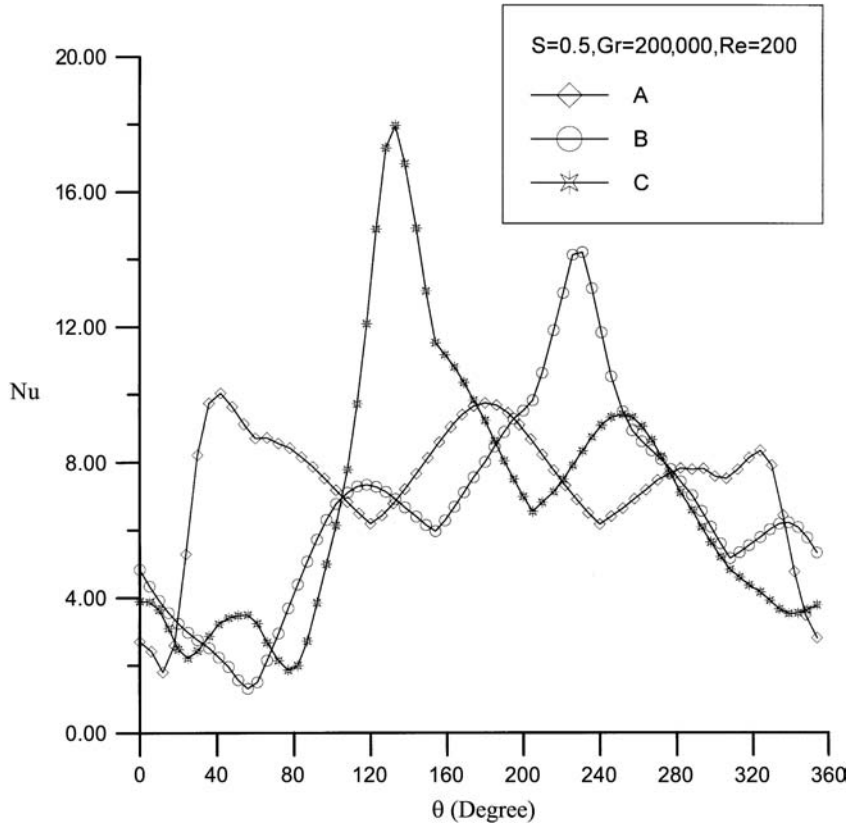

Figure 9.
Time-mean Nusselt number distributions around three cylinders for $Re = 200$ and $Gr = 200{,}000$ at $S = 0.5$

The surface-and time-mean Nusselt number is calculated by the values of time-mean Nusselt number on all nodes of the cylinder boundary. The values of surface-and time-mean Nusselt number for cylinders are listed in Table I for various values of gap spacing ratio with forced convection ($Re = 200$) and mixed convection ($Gr = 80{,}000$ and $200{,}000$ at $Re = 200$). For the flow conditions, the maximum value of surface-and time-mean Nusselt number for cylinders appears at $S = 0.75$, because at this gap distance the values of time-mean Nusselt number are larger and the variations in the distributions are smaller than at other gap spacing from $\theta = 120$ to 240°. This result is caused by a combination of more acceleration due to larger fluid momentum in the gap between cylinders and less deceleration due to smaller friction around the part of cylinders B and C neighboring the wall. At the same gap distance, the value of surface-and time-mean Nusselt number is larger for mixed convection than for forced convection, and it increases with an increase in Grashof number. It is explained from that upward buoyancy effect can make the flow patterns behind the cylinders toward the upper-right surfaces of cylinders and an increase in Grashof number further makes these flow patterns more swinging. The values of surface- and time-mean Nusselt number for cylinders are listed in Table II for various values of gas spacing ratio with mixed convection ($Re = 100$ to 300 at $Gr = 200{,}000$). The values of surface- and time-mean

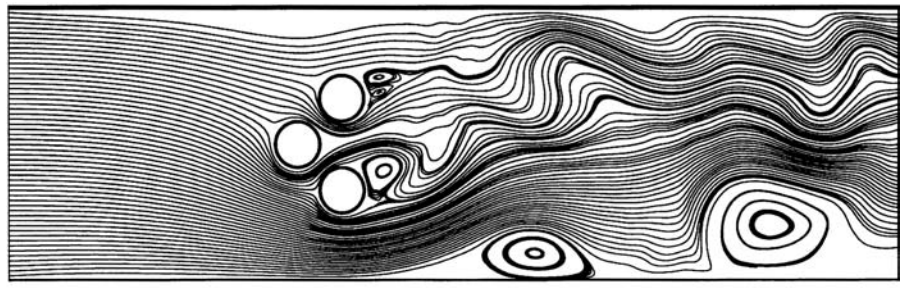

(a)

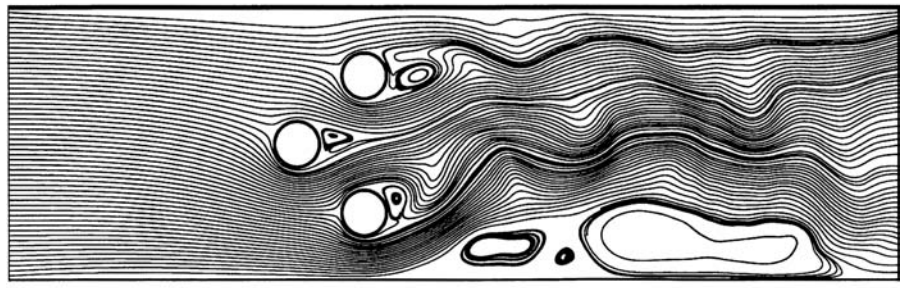

(b)

Figure 10.
Streamlines for $Re = 200$ and $Gr = 200{,}000$: (a) $S = 0.5$ (b) $S = 1.0$ (each time at the peak point of one vortex-shedding cycle)

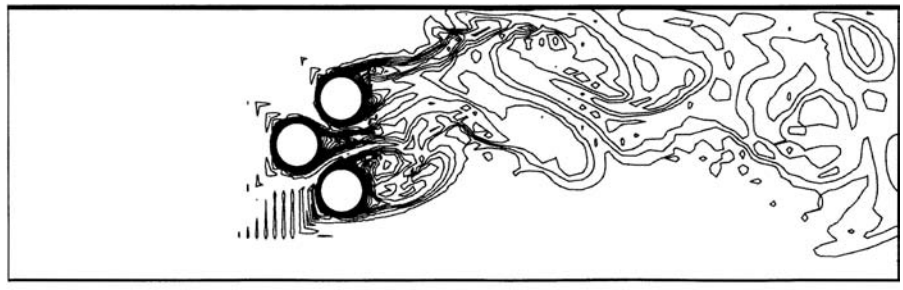

(a)

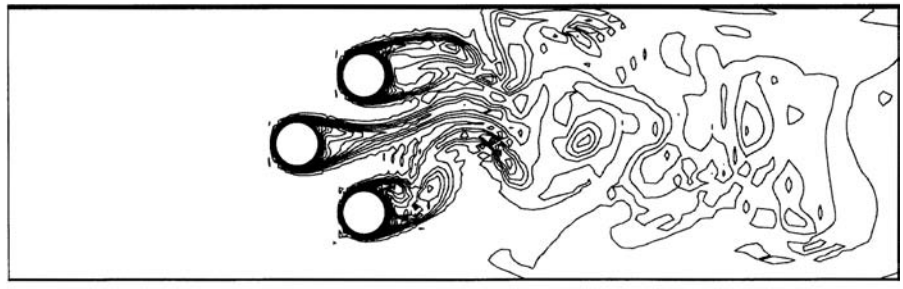

(b)

Figure 11.
Isotherms for $Re = 200$ and $Gr = 200{,}000$ (a) $S = 0.5$ (b) $S = 1.0$ (each time at the peak point of one vortex-shedding cycle)

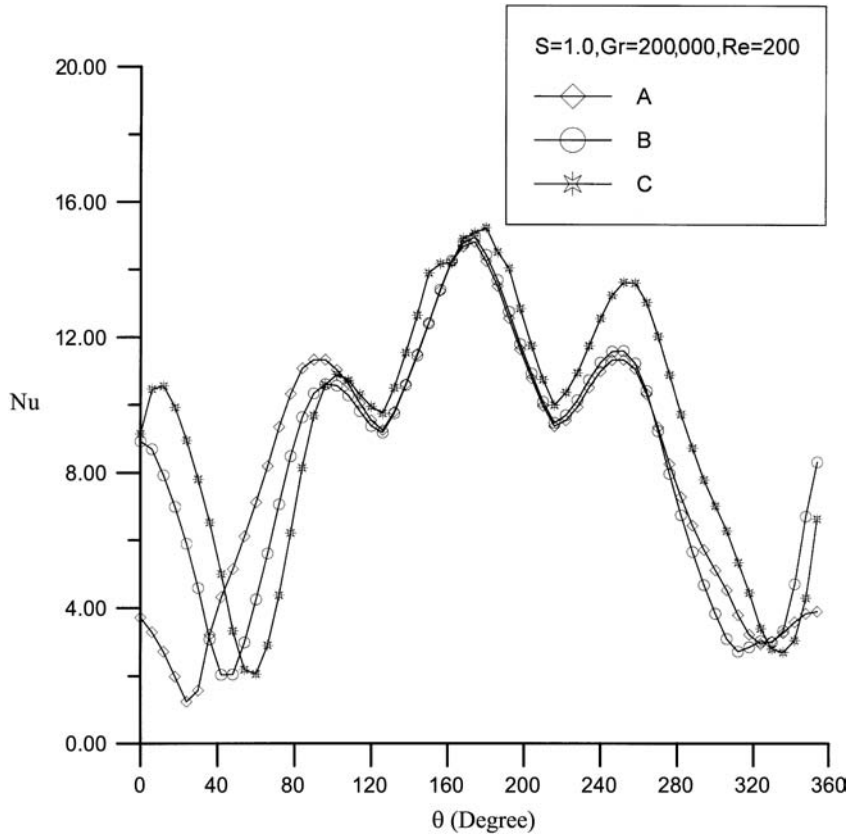

Figure 12.
Time-mean Nusselt number distributions around three cylinders for $Re = 200$ and $Gr = 200{,}000$ at $S = 1.0$

Nusselt number along cylinders increase with increasing Reynolds numbers. The maximum value of surface- and time-mean Nusselt number along cylinders also exists at $S = 0.75$.

6. Conclusions

A projection finite element solution has been obtained on the transient flow and heat transfer for three isothermal cylinders within an adiabatic horizontal channel. Both forced convection and mixed convection of heat transfer are considered. The numerical obtained results further indicated that flow patterns and heat transfer characteristics vary with the Reynolds number, Grashof number and gap-to-diameter ratio. The flow interactions between circular cylinders and channel walls and the distribution of time-mean Nusselt number around three cylinders in a horizontal channel for mixed convection are quite different from those for forced convection. For forced convection, the flow patterns and the distribution of time-mean Nusselt number along the upstream cylinder are symmetric about the front stagnation point. On the contrary, for mixed convection, the flow patterns and the distribution of time-mean Nusselt number

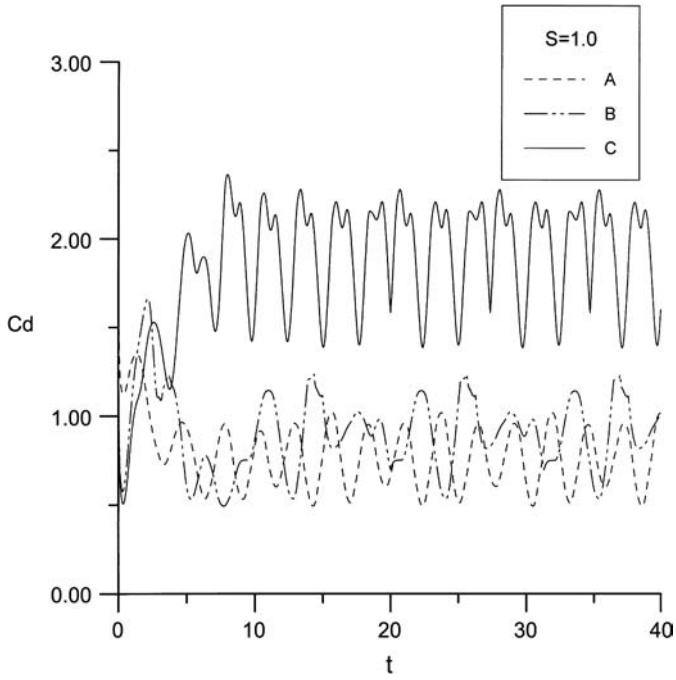

Figure 13.
Drag coefficient C_d vs time for $Re = 200$ and $Gr = 200{,}000$ at $S = 1.0$

	Cylinder A	Cylinder B	Cylinder C
$\overline{Nu}_{avg}$ for forced convection ($Re = 200$)			
$S = 0.5$	6.5538	5.7338	5.7356
$S = 0.75$	7.341	7.6212	7.5835
$S = 1.0$	6.606	7.0893	7.0896
$S = 1.25$	5.4634	6.5032	6.4546
$\overline{Nu}_{avg}$ for mixed convection ($Gr = 80{,}000$, $Re = 200$)			
$S = 0.5$	7.0445	6.2274	6.5794
$S = 0.75$	8.7552	9.1533	9.594
$S = 1.0$	8.0946	8.3964	8.6002
$S = 1.25$	6.2417	7.2397	7.5377
$\overline{Nu}_{avg}$ for mixed convection ($Gr = 200{,}000$, $Re = 200$)			
$S = 0.5$	7.3194	6.6343	6.8669
$S = 0.75$	10.5137	9.6744	9.6124
$S = 1.0$	8.2607	8.4321	9.3345
$S = 1.25$	6.4257	7.0579	7.6744

Table I.
Comparison of surface-and time-mean Nusselt number along cylinders for forced convection ($Re = 200$) and mixed convection ($Gr = 80{,}000$ and 200,000)

along the cylinder are non-symmetric about the front stagnation point because of the upward buoyancy effect. The value of maximum Nusselt number on the upstream cylinder at $S = 1.0$ is larger than that on the upstream cylinder at $S = 0.5$. For mixed convection, at $S = 1.0$, the unsteady vortices behind two downstream cylinders have the tendency toward the upper-right surfaces of cylinders, and the two flow reversals

	Cylinder A	Cylinder B	Cylinder C
$\overline{Nu}_{avg}$ for mixed convection ($Gr = 200{,}000$, $Re = 100$)			
$S = 0.5$	6.6659	5.0136	6.6586
$S = 0.75$	9.7942	8.8623	8.6872
$S = 1.0$	7.0604	7.3081	8.0552
$S = 1.25$	5.6931	6.5871	7.4352
$\overline{Nu}_{avg}$ for mixed convection ($Gr = 200{,}000$, $Re = 200$)			
$S = 0.5$	7.3194	6.6343	6.8669
$S = 0.75$	10.5137	9.6744	9.6124
$S = 1.0$	8.2607	8.4321	9.3345
$S = 1.25$	6.4257	7.0579	7.6744
$\overline{Nu}_{avg}$ for mixed convection ($Gr = 200{,}000$, $Re = 300$)			
$S = 0.5$	7.3616	6.7342	6.9867
$S = 0.75$	10.51369	9.6744	9.6124
$S = 1.0$	8.3203	8.5021	9.5185
$S = 1.25$	6.4961	7.1823	7.7877

Table II. Comparison of surface-and time-mean Nusselt number along cylinders for mixed convection ($Re = 100$ to 300 at $Gr = 200{,}000$)

which occur along the lower channel-wall at $S = 0.5$ are merged into a bigger reversal including two vortices. At the same gap distance, the value of surface-and time-mean Nusselt number is larger for mixed convection than for forced convection, and it increases with an increase in Grashof number. The maximum value of surface- and time-mean Nusselt number along cylinders exists at $S = 0.75$.

References

Chou, J.H. and Chao, S.Y. (1991), "The flow interaction among three circular cylinders", *The Chinese Journal of Mechanics*, Vol. 7, pp. 163-9.

Gowda, Y.T.K, Narayana, P.A.A and Seetharamu, K.N. (1997), "Mixed convection heat transfer past in-line cylinders in a vertical duct", *Numerical Heat Transfer; Part A: Applications*, Vol. 31 No. 5, pp. 551-62.

Horibe, A., Fukusako, S., Yamada, M. and Kawabe, H. (1995), "Forced convection heat transfer characteristics of three cylinders formed across", */ASME/JSME Thermal Engineering Conference*, Vol. 1, pp. 357-62.

Igarashi, T. (1993), "Aerodynamic forces acting on three circular cylinders having different diameters closely arranged in line", *J. Wind Eng. Industrial Aerodynamics*, Vol. 49, pp. 369-78.

Inoue, K. and Hattori, N. (2003), "A numerical study of combined forced and natural convection heat transfer in a vertical cylinder bundle", *Heat Transfer – Asian Research*, Vol. 32 No. 7, pp. 639-49.

Jue, T-C., Wu, H-W. and Hung, S-Y. (2001), "Heat transfer predictions around three heated cylinders between two parallel plates", *Numerical Heat Transfer, Part A*, Vol. 40 No. 7, pp. 715-33.

Kim, S.Y., Hyun, H.J. and Hyun, J.M. (1992), "Mixed convection from multiple-layered boards with corss-streamwise periodic boundary conditions", *International Journal of Heat and Mass Transfer*, Vol. 35, pp. 2941-52.

Kundu, D., Haji-Sheikh, A. and Lou, D.Y.S. (1991), "Pressure and heat transfer in cross flow over cylinders between two parallel plates", *Numerical Heat Transfer, Part A*, Vol. 9, pp. 345-60.

Lacroix, M. and Carrier, R. (1995), "Mixed convection heat transfer from vertically separated horizontal cylinders within confining walls", *Numerical Heat Transfer; Part A: Applications*, Vol. 27 No. 4, pp. 487-98.

Lam, K. and Cheung, W.C. (1988), "Phenomena of vortex shedding and flow interference of three cylinders in different equilateral arrangements", *J. Fluid Mechanics*, Vol. 196, pp. 1-26.

Nakabe, K., Hasegawa, H., Matsubara, K. and Suzuki, K. (1996), "Numerical simulation of combined convection heat transfer from heated cylinder mounted in flow between parallel plates", *Transactions of the Japan Society of Mechanical Engineers*, Vol. 95, pp. 1937-44.

Ramaswamy, B. and Jue, T.C. (1992), "Some recent trends and developments in finite element methods for incompressible thermal flows", *Int. J. Numer. Methods Eng.*, Vol. 35, pp. 671-707.

Tritton, D.J. (1988), *Physical Fluid Dynamics*, Oxford University Press, New York, NY, pp. 21, 164-5.

Wu, H-W. and Perng, S-W. (1999), "Effect of an oblique plate on the heat transfer enhancement of mixed convection over heated blocks in a horizontal channel", *International Journal of Heat and Mass Transfer*, Vol. 42, pp. 1217-35.

Zdravkovic, M.M. (1994), *Flow Around Circular Cylinders*,Vol. 1, Oxford University Press, Oxford.

Žukauskas, A. and Žiugžda, J. (1985) in Hewitt, G.F. (Ed.), *Heat Transfer of a Cylinder in Crossflow*, Springer-Verlag, New York, NY.

Corresponding author
Horng-Wen Wu can be contacted at: z7708033@email.ncku.edu.tw